Manufacturing Rev. 2015, **2**, 19

DOI: 10.1051/mfreview/2015022

**Manufacturing Review**

Available online at:
http://mfr.edp-open.org

RESEARCH ARTICLE OPEN ACCESS

# Material modelling and its application to creep-age forming of aluminium alloy 7B04

Aaron C.L. Lam[1], Zhusheng Shi[1,*], Xia Huang[2], Yo-Lun Yang[1], Yuansong Zeng[2], and Jianguo Lin[1]

[1] Department of Mechanical Engineering, Imperial College London, London SW7 2AZ, UK
[2] AVIC Beijing Aeronautical Manufacturing Technology Research Institute, Beijing 100024, PR China

Received 14 September 2015 / Accepted 21 September 2015

**Abstract –** Creep-ageing behaviour of aluminium alloy 7B04-T651 at 115 °C under a range of tensile stress levels has been experimentally investigated and numerically modelled for creep-age forming (CAF) applications. Creep strain, yield strength evolution and precipitate growth of creep-aged specimens were investigated. The alloy was modelled using a set of unified constitutive equations, which captures its creep deformation and takes into account yield strength contributions from three creep-age hardening mechanisms. Applications of the present work are demonstrated by implementing the determined material model into a commercial finite element analysis solver to analyse CAF operations carried out in a novel flexible CAF tool. Stress relaxation, yield strength, precipitate size and springback were predicted for the creep-age formed plates. The predicted springback were further quantified and compared with experimental measurements and a good agreement of 2.5% deviation was achieved. This material model now enables further investigations of 7B04 under various CAF scenarios to be conducted inexpensively via computational modelling.

**Key words:** Creep-age forming, Material modelling, Process modelling, Aluminium alloy 7B04

## 1. Introduction

Creep-age forming (CAF) is a metal forming technique that utilises the collective behaviour of viscoplastic deformation (creep) and microstructural change (ageing) of aluminium alloys under external loading at elevated temperature [1]. Manufacturing using this technique, in addition to better formed part quality and industrial environment, can reduce the number of manufacturing operations to form a part and thus the associated costs as well [2, 3]. As current deformation of a metallic alloy also depends on its microstructure, which changes dynamically during CAF, accurate prediction of formed part quality cannot be achieved solely using conventional viscoplastic creep equations. Attention has been drawn towards developing mechanism-based creep-ageing constitutive equations that consider evolutions of microstructure and mechanical properties, and efforts have been made towards the concurrent modelling of both the shaping and material processing functions of CAF as a result [3, 4].

In this work, the creep-ageing behaviour of a peak-aged aluminium alloy 7B04 is experimentally investigated and then modelled using a set of unified constitutive equations. The equation set was employed in finite element analysis to simulate an actual CAF process of the alloy in the form of approximately 8-mm-thick plates. Predictions were made for the yield strength evolution, precipitate growth and springback of the physically formed plates. A comparison is made between the simulated and experimentally measured springback values and the springback predictive ability using the material model is briefly discussed. The implications and influences of this work are given at the end of this article.

## 2. Experimental procedure

### 2.1. Material

The material used was aluminium alloy 7B04 whose chemical composition is presented in Table 1. Creep-ageing tensile test pieces of geometry and dimensions shown in Figure 1 and plates of dimensions 600 mm × 350 mm × 8.2 mm had been machined from the same bulk material in the longitudinal rolling orientation and provided in T651 temper by AVIC BAMTRI (Beijing, PR China).

### 2.2. Material testing

Figure 2 illustrates a schematic of the material's heat treatment cycle from solutionising to the subsequent material testing operations. The creep-ageing test procedure used by

*e-mail: zhusheng.shi@imperial.ac.uk

**Table 1.** Chemical composition (wt.%) of 7B04.

| Zn | Mg | Cu | Mn | Fe | Cr | Si | Ni | Ti | Al |
|---|---|---|---|---|---|---|---|---|---|
| 5.97 | 2.48 | 1.51 | 0.33 | 0.16 | 0.16 | 0.07 | <0.05 | <0.05 | Bal. |

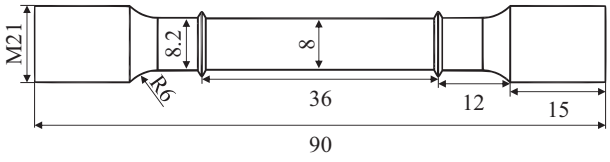


**Figure 1.** Geometry and key dimensions of the test piece (units in mm).

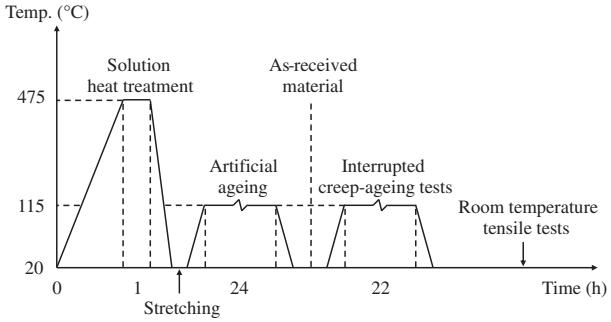


**Figure 2.** Heat treatment history of the material.

Ho et al. [4] was adopted and the tests were carried out at 115 °C under four tensile stress levels: 200, 240, 260 and 280 MPa. Room temperature tensile tests were carried out on selected creep-aged specimens. In addition, samples of the as-received material and those that had received a further 22 h stress-free-ageing were analysed using transmission electron microscopy (TEM) to enable subsequent calibration of the alloy's precipitate growth.

### 2.3. Creep-age forming tests

A novel flexible CAF tool was used for the CAF tests. The tooling setup, as shown in Figure 3, comprised of 25 sparsely spaced forming pins on each side of the top and bottom die holders. Flexible forming surfaces were on both sides of the plate with an additional elastomeric sheet layer between the plate and lower flexible surface. Further details about the method of CAF tool design and test setup can be found in [5] and [6] respectively. The main steps of the forming test include:

1. Setup the forming tool surface by adjusting the heights of forming pins;
2. Load the top die holder to deform the plate to the required shape;
3. Lock the top and bottom die holders using nuts and bolts;
4. Run the creep-ageing thermal cycle;
5. Release the load by loosening the nuts to let springback occur.

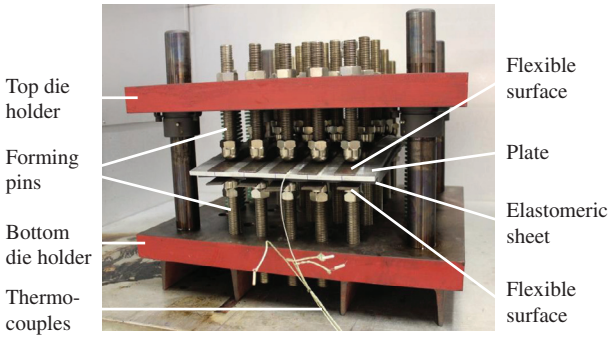


**Figure 3.** Experimental setup for the creep-age forming tests.

CAF tests were carried out on two plates at a single curvature bending radius of 1200 mm. After unloading, profiles of the unloaded plates were measured and springback of the plates ($S$) were calculated using $S = 1 - (\delta_f/\delta_l)$, where $\delta_f$ and $\delta_l$ are the final and loaded centre deflections of each plate respectively. $S$ is a dimensionless quantity and varies from 0 (no springback) to 1 (full springback). Repeated deflection measurements were obtained from each side of the formed plates and the final average value was taken.

## 3. Material modelling

### 3.1. Unified creep-ageing constitutive equations

7B04 is an age-hardenable aluminium alloy. During ageing of 7000-series aluminium alloys, microstructure evolves from supersaturated solid solution and precipitation occurs in the following sequence [7, 8]: Solid solution → GP zones → $\eta'$ → $\eta$ ($MgZn_2$).

The strength of the alloy changes as precipitation takes places. At the early stage, coherent GP zones form and the yield strength increases as precipitates nucleate and grow. GP zones are then gradually replaced by semi-coherent $\eta'$ until a peak-age condition is reached. This is when the alloy attains its peak strength with an optimal precipitate size and density (spacing) combination. Afterwards, $\eta'$ are replaced by incoherent and stable $\eta$ whilst precipitates coarsen, leading to a gradual decrease in strength (over-ageing). Throughout this process, contribution from solid solution hardening gradually decreases and leads to a gradual softening of the alloy. During creep-ageing, dislocation hardening also contributes to the overall strength of the material and shows rapid increase in the early stage.

In order to model the described behaviour of 7B04, the multiaxial unified constitutive equations proposed by Zhan et al. [9] were adapted:

$$\dot{\varepsilon}_e^{cr} = A_1 \sinh\{B_1[\sigma_e(1-\overline{\rho}_d) - k_{\varepsilon c}\sigma_y]\} \quad (1)$$

**Table 2.** Initial conditions used for CAF of 7B04-T651 (115 °C, 22 h).

| $\sigma^0_{sol}$ (MPa) | $\sigma^0_{age}$ (MPa) | $\sigma^0_y$ (MPa) | $\bar{r}^0_p$ | $\bar{\rho}^0_d$ |
|---|---|---|---|---|
| 190 | 347 | 537 | 1 | 1E-5 |

**Table 3.** Material constants determined for CAF of 7B04-T651 (115 °C, 22 h).

| $A_1$ ($h^{-1}$) | $B_1$ ($MPa^{-1}$) | $k_{ec}$ | $C_a$ (MPa) | $m_1$ | $C_s$ (MPa) | $m_2$ | $A_2$ (MPa) | $n_d$ |
|---|---|---|---|---|---|---|---|---|
| 1.95E-6 | 0.042 | 0.16 | 4 | 0.9 | 0.2 | 0.45 | 260 | 0.7 |
| $C_r$ ($h^{-1}$) | $Q_r$ | $m_3$ | $\gamma_r$ | $m_4$ | $A_3$ | $C_\rho$ ($h^{-1}$) | $m_5$ | |
| 0.098 | 1.8 | 2.2 | 3 | 2 | 150 | 0.145 | 1.5 | |

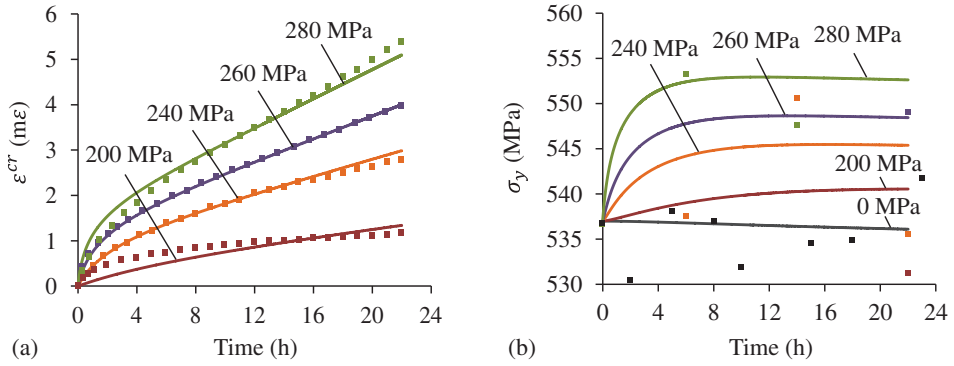


**Figure 4.** Comparisons of the experimentally obtained (symbols) and calibrated (solid lines) (a) creep-ageing curves and (b) yield strength evolutions for creep-ageing at 115 °C under the indicated stress levels.

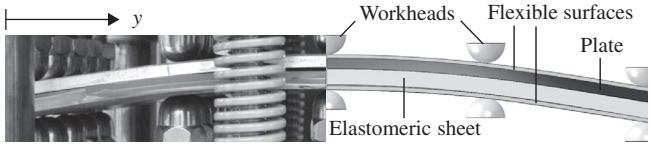


**Figure 5.** Side-view images taken at full loading of (a) a physical forming test and (b) finite element simulation with to-scale rendering of shell thicknesses.

$$\dot{\sigma}_{age} = C_a \dot{\bar{r}}_p^{\,m_1}(1-\bar{r}_p) \tag{2}$$

$$\dot{\sigma}_{sol} = -C_s \dot{\bar{r}}_p^{\,m_2}\left|\bar{r}_p - 1\right| \tag{3}$$

$$\dot{\sigma}_{dis} = A_2 \cdot n_d \cdot \bar{\rho}_d^{\,n_d-1}\dot{\bar{\rho}}_d \tag{4}$$

$$\sigma_y = \sigma_{sol} + \sqrt{\sigma^2_{age} + \sigma^2_{dis}} \tag{5}$$

$$\dot{\bar{r}}_p = C_r\left(Q_r - \bar{r}_p\right)^{m_3}\left(1 + \gamma_r \bar{\rho}_d^{\,m_4}\right) \tag{6}$$

$$\dot{\bar{\rho}}_d = A_3(1-\bar{\rho}_d)\dot{\varepsilon}^{cr}_e - C_\rho \bar{\rho}_d^{\,m_5} \tag{7}$$

where $A_1$, $B_1$, $k_{ec}$, $C_a$, $m_1$, $C_s$, $m_2$, $A_2$, $n_d$, $C_r$, $Q_r$, $m_3$, $\gamma_r$, $m_4$, $A_3$, $C_\rho$, $m_5$ are material constants. The normalised dislocation density is given by $\bar{\rho}_d = (\rho - \rho_i)/\rho_m$, where $\rho_i$ and $\rho_m$ are respectively the dislocation density of the virgin material and the maximum (saturated) dislocation density. The normalised radius of precipitate is defined as $\bar{r}_p = r/r_c$, where $r$ and $r_c$ are the current and peak-aged precipitate size respectively. Equations (1)–(7) describe the inter-relationship amongst the equivalent stress ($\sigma_e$), normalised dislocation density ($\bar{\rho}_d$), normalised radius of precipitate ($\bar{r}_p$) and effective creep strain ($\varepsilon^{cr}_e$), as well as the strength contributions from solid solution hardening ($\sigma_{sol}$), age hardening ($\sigma_{age}$) and dislocation hardening ($\sigma_{dis}$). Equation (1) describes the rate of creep strain accumulation, which is not only a function of stress but also of dislocation density and yield strength ($\sigma_y$). Readers are referred to [9] for detailed descriptions of Equations (1)–(7).

### 3.2. Determination of material constants

An evolutionary-algorithm-based optimisation software developed by Zhang et al. [10] was used for material constants determination. The alloy's yield strength evolutions and creep-ageing curves obtained from the tensile creep-ageing tests were used for model calibration. This was coupled with manual constants adjustments carried out in MATLAB to calibrate for the TEM analysis result.

Tables 2 and 3 present respectively the initial conditions used and the material constants determined. Referring to the

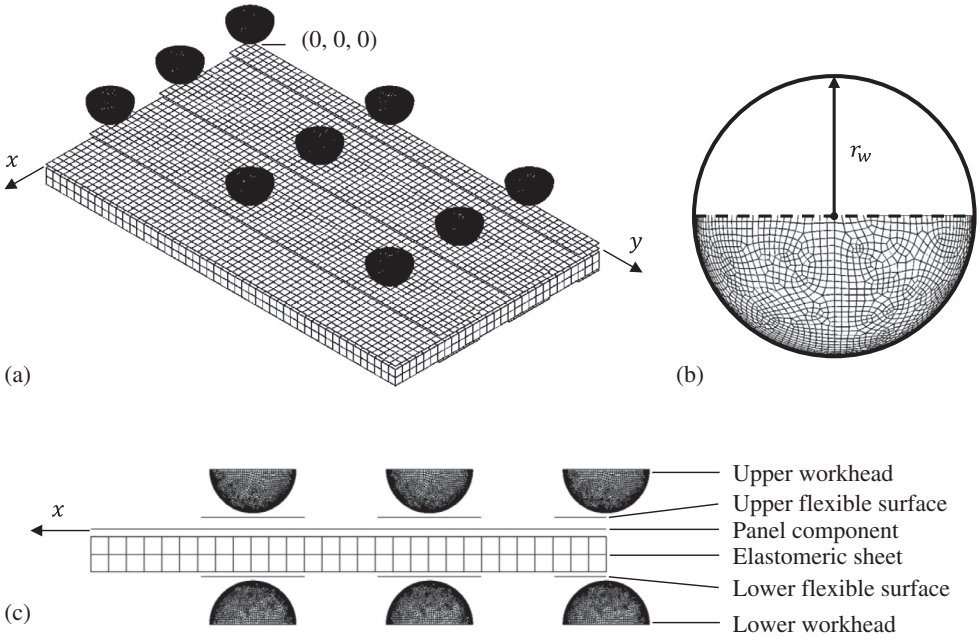


**Figure 6.** (a) Isometric view of the finite element model; (b) Finite element mesh of a workhead with an arbitrary revolving axis (dashed line) and the radius of revolvement; (c) *xz* plane view of the finite element model with the different parts illustrated. Adapted from [6].

initial conditions, the as-quenched yield strength of 7B04 was 206 MPa [11]. A value of $\sigma^0_{\text{sol}} = 190$ MPa was chosen for the as-recieved T651 condition. Before any creep-ageing takes place, zero dislocation hardening was assumed and thus $\sigma^0_{\text{age}} = \sigma^0_y - \sigma^0_{\text{sol}}$, where $\sigma^0_y = 537$ MPa was obtained from the tensile tests. $\bar{r}^0_p = 1$ was set as the material is at its peak-aged condition. The initial dislocation density is significantly smaller than the maximum dislocation density and $\bar{\rho}^0_d = 1\text{E-}5$ was used.

Figure 4 illustrates a comparison for each of the calibrated creep-ageing curves and yield strength evolutions with the corresponding experimental data. After 22 h of creep-ageing, maximum deviations of 0.29 mε and 9.35 MPa are observed which represent a 5.6 and 1.8% difference respectively. Thus, characteristics of both the viscoplastic deformation and yield strength evolution of 7B04-T651 during creep-ageing have been captured with close agreements. In addition to the creep and strength evolutions, the alloy's precipitate growth was also calibrated. This was based on the TEM analysis result which estimated an average growth in precipitate radius from 8.5 to 12.6 nm after 22 h of stress-free-ageing.

## 4. Application of the material model to finite element modelling of creep-age forming

### 4.1. Finite element model

In order to demonstrate the application of the material model to CAF process, a finite element (FE) model that represents a quarter of the flexible CAF tool was constructed in Abaqus. As shown in Figure 5, only workheads of the forming pins were modelled. Detailed descriptions of the FE model and modelling procedure are available in [6], whilst the influences of residual stresses and initial distortion of plates on springback prediction are not considered in this study.

For completion, the FE model used in this study is briefly described here. Mesh convergence studies were carried out following a one-mesh-at-a-time principle whereby the convergences of the flexible surfaces, elastomeric sheet and panel component were individually assessed. Figure 6 illustrates the final condition of the FE meshes. The workheads were assumed to be perfectly spherical with a radius of $r_w = 14.65$ mm and modelled as rigid bodies. The plates were modelled using initially flat shell elements with their actual plate thicknesses, a Young's modulus ($E$) of 67 GPa, a Poisson's ratio ($\nu$) of 0.33 and a thermal expansion coefficient ($\alpha$) of 2.3E-5 $K^{-1}$ assigned. Equations (1)–(7) were implemented into Abaqus via the user-defined subroutine CREEP with the initial conditions and material constants in Tables 2 and 3 assigned. The flexible surfaces were modelled as spring-tempered steel with $E = 210$ GPa, $\nu = 0.3$ and $\alpha = 1.3\text{E-}5$ $K^{-1}$. The elastomeric sheet has $\alpha = 2.5\text{E-}5$ $K^{-1}$ and was modelled as an isotropic hyperelastic material and assigned with parameters equivalent to those of a 60 Shore A hardness elastomer. The following six-step modelling procedure was employed:

1. Initiate the simulation with temperature, boundary conditions and contact scheme defined;
2. Load the upper workheads to deform the plate whilst the lower workheads remain fixed;
3. Heat the entire configuration up to the CAF temperature;
4. Propagate into a visco step for creep-ageing to take place;
5. Cool the entire configuration down to room temperature;
6. Unload the upper workheads to allow springback to occur.

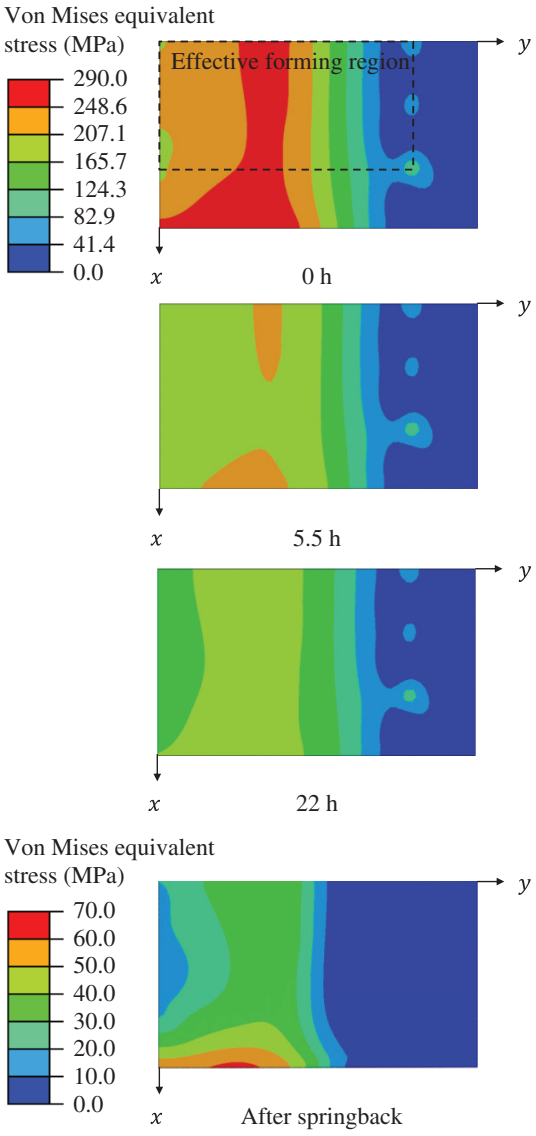


**Figure 7.** Evolution of von Mises equivalent stress at 0, 5.5 and 22 h of the creep-ageing time and the final stress distribution after springback. Distributions are plotted for the topmost tensile surface of a quarter 8.2-mm-thick plate at a single curvature bending radius of 1200 mm under 115 °C. The dashed line illustrates the effective forming region of the flexible form tool.

Simulations of the CAF tests were carried out using the FE model under conditions that match those of the forming tests. Stress relaxation, yield strength evolution, precipitate growth and springback of the plates were modelled and analysed, with the springback further quantified and compared with those of the physically formed plates.

### 4.2. Stress relaxation

Figure 7 shows the stress relaxation that occurred on the topmost tensile surface of a quarter (300 mm × 175 mm) 8.2-mm-thick plate during CAF in the flexible form tool. Three field plots were recorded at the 0 (at an infinisimal first numerical time increment), 5.5 and 22 h (the total creep-ageing time) time points of the creep-ageing period. The final plot illustrates the stress distribution after springback.

The physical flexible form tool has an effective forming region (EFR) of 480 mm × 240 mm, which translates to a 240 mm × 120 mm region from the centre point of symmetries of the quarter model. When the plate is fully loaded at 0 h, a higher overall stress state is observed in the region between the $y = 0$ and 120 mm workheads. The maximum stress level is observed outside the EFR at $x = 175$ mm. This is due to the act of Poisson's effect on the plate region where it is unconstrained (outside the EFR), which as a result introduces a greater presence of transverse strain to the region, increasing the overall stress level there. In that region, a maximum stress relaxation of 102 MPa was recorded, reducing the stress level there from 288.2 to 186.2 MPa over the 22 h period. Sixty-eight percent of the 102 MPa stress relaxation took place within the first 5.5 h of creep-ageing.

In general, the overall stress state decreases gradually with increasing $y$ and the minimum stress level is observed outside the EFR. Local stress concentrations can be observed at the $x$-border of the EFR, somewhere between $y = 200$ and 300 mm, which is at the proximity of where the $y = 240$ mm workheads are located. Because internal stresses of the plate were not fully relaxed by the 22 h of creep-ageing, the plate springs back upon tool unloading due to elastic stress recovery. After springback, the region of high stress relaxation outside the EFR has the highest amount of residual stress on the plate surface; about four times lower than the stress level when the plate was fully loaded. Within the EFR, distribution of the stress field is similar to that of the plate immediately before unloading, but with approximately five times less in the magnitude of stress.

### 4.3. Yield strength prediction

Figure 8a shows the field plots of yield strength evolution for the topmost tensile surface of the same plate during CAF. At 0 h, the plate is deformed elastically and the yield strength throughout the plate has an expected initial value of 537 MPa. Due to the different stress levels experienced by the plate at different regions, differences in the rate of yield strength evolution over the area of the plate begin to emerge with time. A higher strength region is observed at approximately $y = 90$ mm, which correlates with the high stress region in Figure 7. Within this region, the yield strength of the material has grown from 537 MPa to a median value of 540 MPa after 5.5 h. At 5.5 h, the yield strength gradually decreases in a $y$-outward manner, agreeing with the stress distributions and their relationship defined by the material model. Outside the EFR in the $y$ direction is a region of the plate where stress-free-ageing occurs most and a 0.2 MPa minor softening of the material is observed.

Under the CAF condition investigated and of the three discrete time points captured, the overall material's yield strength is highest at 5.5 h, leading to an overall trend of softening over the whole plate area from then onwards.

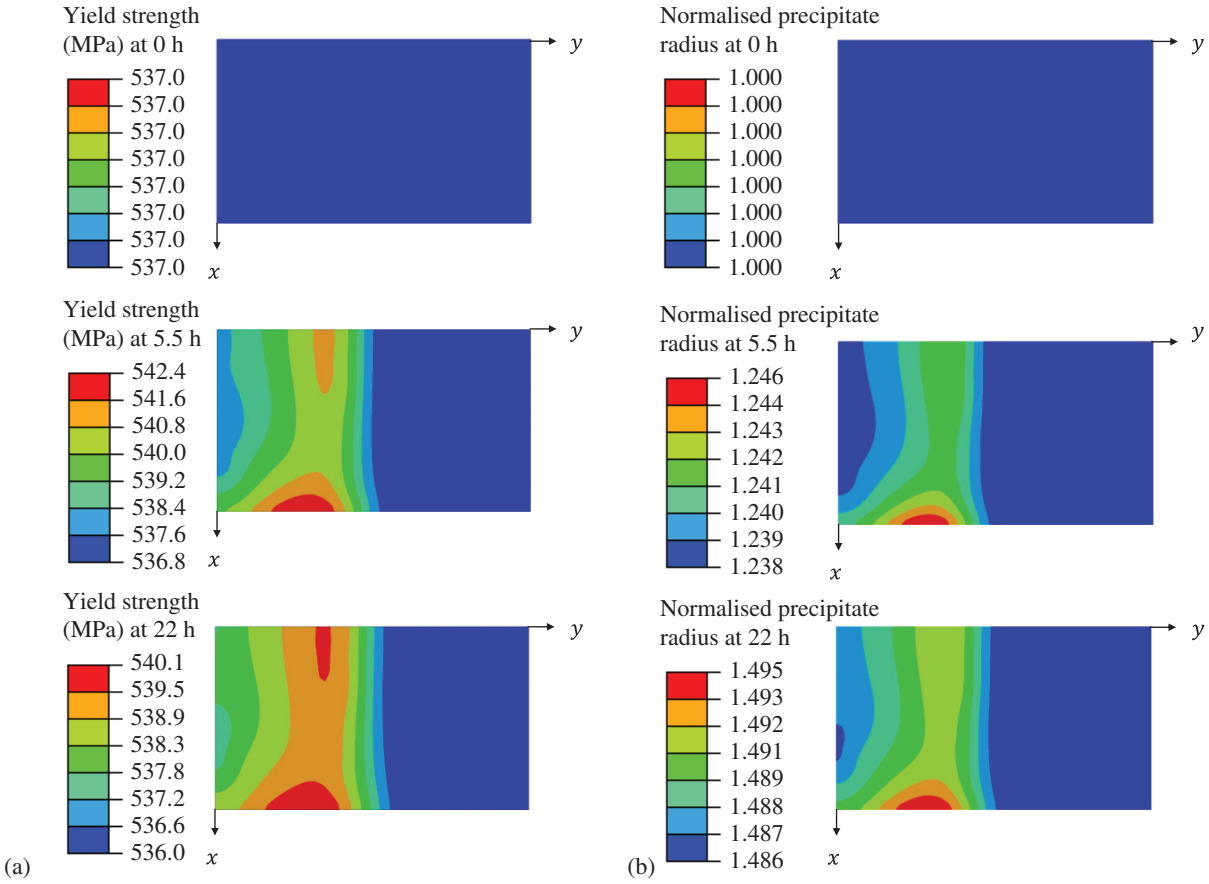


**Figure 8.** Evolutions of (a) yield strength and (b) normalised precipitate radius at the topmost tensile surface of a quarter 8.2-mm-thick plate at a single curvature bending radius of 1200 mm during CAF under 115 °C.

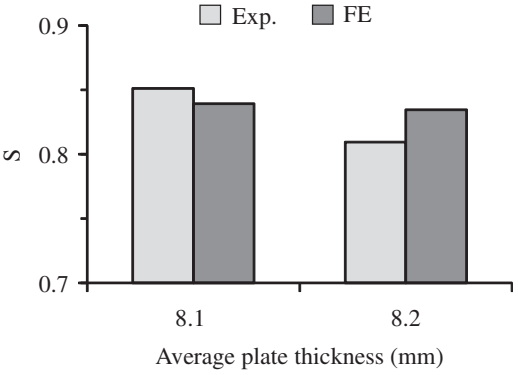


**Figure 9.** Comparison of the experimentally measured and FE-simulated springback of 7B04-T651 plates. The forming tests were conducted at a single curvature bending radius of 1200 mm under 115 °C for 22 h.

At the end of the CAF process, the median strength value of the plate in the high strength region has reduced from the 540 MPa at 5.5 h to 538.3 MPa at 22 h. For the outer $y$ region where the stress levels are negligible, the yield strength of the plate has softened further by 0.8 MPa, to a final value of 536 MPa.

### 4.4. Precipitate size prediction

Figure 8b shows the field plots of normalised precipitate radius for the same plate and arranged in the same format as those illustrated in Figure 8a. In general, the field plots show a similar precipitate growth trend as those recorded for the yield strength evolution in Figure 8a. This is because the hardening mechanisms of CAF (Eqs. (2)–(5)) are dependent on precipitate size, dislocation density and their inter-relationship, which in turn, are influenced by the stress levels experienced and therefore the creep strain rate of the plate. On the other hand, unlike yield strength which has mechanisms that activate the softening of the material and led to a decrease in its value, the precipitate radius of the alloy has grown steadily over the entire course of creep-ageing time. Within the first 5.5 h of strength growth period, the median $\bar{r}_p$ value has increased by 24% from 1.000 to 1.241. Over-creep-ageing of the alloy from its peak strength value occurred at some point within the next 16.5 h period, during which a further 20% increase in the median precipitate radius value, from 1.241 to 1.489, is observed.

### 4.5. Springback prediction and comparison

Figure 9 illustrates a comparison between the measured and FE-simulated springback values. The FE-simulated

springback value is lower than the experimental value for the 8.1-mm-thick plate whilst the opposite is observed for the 8.2-mm-thick plate. Based on the FE-simulated results which show a 0.4% difference between the two plates, it can be concluded that the springback sensitivity to a 0.1 mm difference in plate thickness is close to negligible under the current CAF condition. Therefore, the 4.2% difference between the experimental springback values of the two plates is likely to be due to experimental uncertainties, which may include their difference in residual stress level and initial plate distortion prior to CAF submission [6]. Nonetheless, the measured and FE-simulated results both show a decrease in springback as the plate thickness increases from 8.1 to 8.2 mm. The FE-simulated springback values deviate slightly from the experimental values but they are within an acceptable range of −1.2 and +2.5% difference in springback or +0.3 and −0.6 mm difference in vertical deflection. Thus, a good prediction of springback was achieved using this material model.

## 5. Summary

A material model was presented with its constants determined for creep-age forming of aluminium alloy 7B04-T651. In addition to creep deformation, the model also predicts the precipitate growth and yield strength evolution of the alloy. Its applications to creep-age forming have been demonstrated through the analyses of stress relaxation, yield strength evolution, precipitate growth and springback using finite element modelling techniques. A good agreement of 2.5% deviation from the physical forming test results was achieved for the predicted springback values.

## Implications and influences

Due to the long processing hours required for creep-age forming, the technique is often found associated with the production of extra-large panel components such as aircraft wing skin panels. As a result, the quality of a creep-age formed part, largely determined by its final shape, strength specification and condition of microstructure, can vary greatly within the large area covered by the component. Full experimental investigations are time consuming to perform and also highly costly. The test programme, material modelling techniques and their applications summarised in this article enable creep-age forming of aerospace-grade alloys, under various initial, boundary and loading conditions, to be investigated inexpensively via computational modelling. Cost-efficient and accurate investigations can now be performed for creep-age forming of aluminium alloy 7B04-T651, enabling further advancement of the forming technique and its associated technologies.

*Acknowledgements.* The strong support from Aviation Industry Corporation of China (AVIC) Beijing Aeronautical Manufacturing Technology Research Institute (BAMTRI) for this funded research is much appreciated. The research was performed at the AVIC Centre for Structural Design and Manufacture at Imperial College London.

## References

1. M.C. Holman, Autoclave age forming large aluminium aircraft panels, Journal of Mechanical Working Technology 20 (1989) 477–488.
2. F. Eberl, S. Gardiner, G. Campanile, G. Surdon, M. Venmans, P. Prangnell, Ageformable panels for commercial aircraft, Journal of Aerospace Engineering 222 (2008) 873–886.
3. L. Zhan, J. Lin, T.A. Dean, A review of the development of creep age forming: Experimentation, modelling and applications, International Journal of Machine Tools and Manufacture 51 (2011) 1–17.
4. K.C. Ho, J. Lin, T.A. Dean, Constitutive modelling of primary creep for age forming an aluminium alloy, Journal of Materials Processing Technology 153–154 (2004) 122–127.
5. A.C.L. Lam, Z. Shi, J. Lin, X. Huang, Y. Zeng, T.A. Dean, A method for designing lightweight and flexible creep-age forming tools using mechanical splines and sparse controlling points, International Journal of Advanced Manufacturing Technology 80 (2015) 361–372.
6. A.C.L. Lam, Z. Shi, J. Lin, X. Huang, Influences of residual stresses and initial distortion on springback prediction of 7B04-T651 aluminium plates in creep-age forming, International Journal of Mechanical Sciences 103 (2015) 115–126.
7. R. Ferragut, A. Somoza, A. Tolley, Microstructural evolution of 7012 alloy during the early stages of artificial ageing, Acta Materialia 47 (1999) 4355–4364.
8. G. Sha, A. Cerezo, Early-stage precipitation in Al-Zn-Mg-Cu alloy (7050), Acta Materialia 52 (2004) 4503–4516.
9. L. Zhan, J. Lin, T.A. Dean, M. Huang, Experimental studies and constitutive modelling of the hardening of aluminium alloy 7055 under creep age forming conditions, International Journal of Mechanical Sciences 53 (2011) 595–605.
10. P. Zhang, J. Lin, D. Balint, OPT-CAF: the optimisation tool for calibrating creep constitutive equations, Project report, Imperial College London, 2012.
11. Z. Li, B. Xiong, Y. Zhang, B. Zhu, F. Wang, H. Liu, Microstructural evolution of aluminum alloy 7B04 thick plate by various thermal treatments, Transactions of Nonferrous Metals Society of China 18 (2008) 40–45.

**Cite this article as**: Lam ACL, Shi Z, Huang X, Yang YL, Zeng Y & Lin J: Material modelling and its application to creep-age forming of aluminium alloy 7B04. Manufacturing Rev. 2015, **2**, 19.